Research
A SCIENCE PARTNER JOURNAL

RESEARCH ARTICLE

Structural Pharmacology of Bufotenine Derivatives in Activating the 5-HT$_{1A}$ Receptor for Therapeutic Potential in Depression and Anxiety

Shu-jie Li[1,2,3†], Qing-ning Yuan[1,3†], Wen-yuan Wu[1†], Zhi-han Chen[1], Duo Chen[1], Hong Shan[3], Qin-yu Chu[4], Wen Hu[3], Kai Wu[3], Tao Liu[3], Yu-yu Zhu[1], Li Hou[3], Jing Zhou[1*], Jia Duan[3*], Jin-ao Duan[1*], H. Eric Xu[3*], and Hong-yue Ma[1*]

[1]Jiangsu Collaborative Innovation Center of Chinese Medicinal Resources Industrialization and Jiangsu Key Laboratory for High Technology Research of TCM Formulae, College of Pharmacy, Nanjing University of Chinese Medicine, Nanjing 210023, China. [2]Department of Traditional Chinese Medicine, Fujian Medical University Union Hospital, Fuzhou 350000, Fujian, China. [3]State Key Laboratory of Drug Research, Shanghai Institute of Materia Medica, Chinese Academy of Sciences, Shanghai 201203, China. [4]School of Pharmaceutical Science and Technology, Hangzhou Institute for Advanced Study, UCAS, Hangzhou 310024, China.

*Address correspondence to: zhoujing@njucm.edu.cn (J.Z.); duanjia@simm.ac.cn (Jia Duan); dja@njucm.edu.cn (Jin-ao Duan); Eric.Xu@simm.ac.cn (H.E.X.); hongyuema@njucm.edu.cn (H.M.)
†These authors contributed equally to this work.

Citation: Li S, Yuan Q, Wu W, Chen Z, Chen D, Shan H, Chu Q, Hu W, Wu K, Liu T, et al. Structural Pharmacology of Bufotenine Derivatives in Activating the 5-HT$_{1A}$ Receptor for Therapeutic Potential in Depression and Anxiety. *Research* 2025;8:Article 0987. https://doi.org/10.34133/research.0987

Submitted 17 August 2025
Revised 20 October 2025
Accepted 23 October 2025
Published 23 December 2025

Copyright © 2025 Shu-jie Li et al. Exclusive licensee Science and Technology Review Publishing House. No claim to original U.S. Government Works. Distributed under a Creative Commons Attribution License (CC BY 4.0).

The 5-HT$_{1A}$ receptor is a critical target in the treatment of depression and anxiety. Bufotenine derivatives, such as 5-methoxy-*N*,*N*-dimethyltryptamine (5-MeO-DMT), 5-hydroxy-*N*,*N*-dimethyltryptamine (5-OH-DMT), and 5-hydroxy-*N*,*N*,*N*-dimethyltryptamine—derived from traditional Chinese medicine—have shown antidepressant potential. However, the structural basis of their interaction with 5-HT$_{1A}$ and their pharmacological profiles remain incompletely understood. This study investigated bufotenine derivatives acting on multiple serotonin receptors, highlighting 5-HT$_{1A}$ as a key mediator of antidepressant effects while recognizing 5-HT$_{2A}$ as primarily responsible for hallucinogenic outcomes, to identify candidates with therapeutic efficacy but reduced hallucinogenic liability. We determined the cryo-electron microscopy structures of 5-HT$_{1A}$ bound to selected bufotenine derivatives. Functional assays in mice, including behavioral tests and receptor activation studies, were used to evaluate the antidepressant of each compound. Structural analysis revealed that all bufotenine derivatives engage conserved motifs within the 5-HT$_{1A}$ binding pocket, with 5-OH-DMT displaying a distinct interaction pattern. Behavioral assays showed that 5-OH-DMT and 5-MeO-DMT retained strong antidepressant and anxiolytic effects. These pharmacological differences correlate with their unique receptor binding conformation. This study delineated the structural pharmacology of bufotenine derivatives at the 5-HT$_{1A}$ receptor, identifying 5-OH-DMT and 5-MeO-DMT as promising antidepressant and anxiolytic candidates. The findings establish a molecular framework for the development of next-generation nonhallucinogenic therapeutics aimed at 5-HT$_{1A}$.

Introduction

Depression is a prevalent mental illness that affects the quality of life and psychosocial performance. It causes depression, anhedonia, poor self-esteem, guilt, worthlessness, weariness, sleep problems, and suicidal thoughts [1,2]. Standard antidepressants like monoamine oxidase inhibitors and selective serotonin reuptake inhibitors regulate central nervous system monoamine neurotransmitter levels. The therapeutic effects of these drugs usually take weeks to appear [3]. About two-thirds of patients relapse or do not respond to these treatments [4,5]. The monoamine hypothesis, which states that neurotransmitter imbalances in serotonin (5-HT), norepinephrine, and dopamine cause depression, underpins the efficacy and pharmacodynamics of first- and second-generation antidepressants [6,7]. Depressive disorders may be caused by at least 6 serotonin receptor subtypes (5-HT$_{1A}$, 5-HT$_{1B}$, 5-HT$_{1D}$, 5-HT$_{2A}$, 5-HT$_{2C}$, and 5-HT$_{7}$), according to emerging evidence [8,9].

Serotonin dysregulation is largely considered a key cause of severe depressive illness. The neuropathology of depression depends on the 5-HT$_{1A}$ receptor (5-HT$_{1A}$R), the main serotonin receptor [10,11]. 5-HT$_{1A}$R regulates melancholy and anxiety [12]. In mice, 5-HT$_{1A}$R-deficient animals exhibit increased anxiety, dread, and freezing, demonstrating its function in anxiety

regulation [13]. In addition, overexpression of 5-HT_{1A}R in the forebrain during early postnatal development, but not in the raphe nuclei, restores conventional behavioral features in knockout mice, underscoring the importance of postsynaptic 5-HT_{1A}R in mental health [14]. Mice and primates with reduced 5-HT_{1A}R expression exhibit anxiety and stress-related behaviors [15,16]. Both psychedelics and selective 5-HT_{1A}R agonists exhibit anxiolytic properties through distinct yet partly overlapping mechanisms. Clinically used 5-HT_{1A} agonists such as buspirone alleviate anxiety by modulating serotonergic signaling and stress-coping pathways. Psychedelics like psilocybin, which also engage 5-HT_{1A}Rs alongside 5-HT_{2A} activation, demonstrate additional anxiolytic and antidepressant potential. 5-HT_{1A}R is a target of licensed anxiolytic and antidepressant drugs including buspirone (BuSpar) [17] and vilazodone (Viibryd) [18]; therefore, knowing its processes is crucial to improving depression therapies. Through Gi/o family heterotrimeric G proteins, 5-HT_{1A}R inhibits adenylyl cyclase and lowers cyclic adenosine monophosphate (cAMP) levels, and this effect is enhanced by 5-HT_{1A}R agonists [19]. Despite extensive investigation, the molecular abnormalities in the serotonin pathway linked to clinical depression and suicidality are still unknown.

Traditional antidepressants have limited effectiveness, extensive treatment times, and lasting adverse effects, underscoring the need for innovative and fast-acting treatments [20–22]. Psychoactive bufotenine compounds from *Bufo alvarius* toad parotid glands affect humans and animals. Bufotenine, a natural tryptamine in Ch'an Su, has been utilized in Chinese medicine for centuries [23]. Bufotenine derivatives have an indole core, an amino group, and an ethyl side chain like serotonin. These derivatives include 5-methoxy-*N*,*N*-dimethyltryptamine (5-MeO-DMT), 5-hydroxy-*N*,*N*-dimethyltryptamine (5-OH-DMT), and 5-hydroxy-*N*,*N*,*N*-dimethyltryptamine (5-OH-TMT). Studies reveal that indole ring alterations at position 5 increase potency relative to that of other substituted and unsubstituted tryptamines [24], but clinical effects are similar [25]. Recent discoveries that hallucinogens may treat depression, anxiety, drug use disorders, and obsessive-compulsive behaviors have increased interest in their pharmacology [26,27]. Some tryptamines, both 5-MeO-substituted and unsubstituted, block or release 5-HT [28]. This combined mechanism of 5-HT reuptake inhibition and receptor interaction may be better than selective serotonin reuptake inhibitors for mood disorders [29]. Most structure–activity relationship research on tryptamines has concentrated on indole ring replacements, with few investigations on terminal amino group modifications [30]. Some 5-MeO-tryptamines bind with the 5-HT_{2A} receptor (5-HT_{2A}R), although they usually work better at 5-HT_{1A}R [31,32]. However, inconsistent results have been reported [28]. Additionally, bufotenine derivatives' 5-HT_{1A}R modulation effect in depression therapy is unknown.

Extensive research has established that psychedelics function as 5-HT_{2A}R agonists, capable of inducing profound alterations in perception, cognition, and mood states [33]. However, emerging evidence suggests that the therapeutic efficacy of 5-HT_{2A}R agonists may not necessarily depend on psychedelic experiences, with studies demonstrating that psilocybin's antidepressant effects can occur independently of both 5-HT_{2A}R activation and associated psychedelic activity [9,34,35]. These findings highlight a critical knowledge gap regarding the mechanistic relationship between psychedelic properties and therapeutic outcomes in 5-HT_{2A}R-targeted interventions. The clinical translation of psychedelic-based therapies faces substantial methodological and practical challenges. The compounds' intrinsic psychoactive properties fundamentally undermine the integrity of double-blind clinical trial designs, while the standard practice of combining pharmacological intervention with psychotherapy obscures the precise attribution of therapeutic benefits. Additional concerns regarding long-term safety profiles and potential for non-medical use further complicate their clinical implementation. Motivated by increasing scientific interest in microdosing protocols for cognitive enhancement and mood regulation [36], we sought to develop a novel therapeutic agent that maintains robust antidepressant efficacy while exhibiting minimized psychedelic properties, thereby addressing current limitations in the field.

This study explored the structural and functional mechanisms of how bufotenine derivatives, namely, 5-MeO-DMT, 5-OH-DMT, and 5-OH-TMT, bind to and activate 5-HT_{1A}R at molecular and atomic levels. Furthermore, we systematically investigated the therapeutic potential of bufotenine derivatives in established mouse models of depression. Our study shows that 5-OH-DMT acts on multiple serotonin receptors, with 5-HT_{1A} contributing to its antidepressant and anxiolytic effects and reduced 5-HT_{2A} involvement accounting for diminished hallucinogenic activity. These results provide a pharmacological foundation for the development of next-generation antidepressant therapies with targeted 5-HT_{1A}R engagement.

Results

Bufotenine derivatives acting at 6 depression-related serotonin receptors

We evaluated the impact of bufotenine derivatives on 6 serotonin receptor subtypes associated with depression (5-HT_{1A}, 5-HT_{1B}, 5-HT_{1D}, 5-HT_{2A}, 5-HT_{2C}, and 5-HT_{7}) using the GloSensor cAMP assay to measure Gi and Gs activation and the IP-One assay to assess Gq activation, thereby detecting signaling activity at each receptor. All synthesized bufotenine derivatives demonstrated potency at 5-HT receptor subtypes, with particularly pronounced potency and efficacy observed at 5-HT_{1A}Rs (Fig. 1A). 5-OH-DMT demonstrated the greatest potency for 5-HT_{1A}R with an EC_{50} of 0.1 μM. The activation potency at 5-HT_{1A}R was lower for 5-MeO-DMT (EC_{50} = 0.5 μM) and 5-OH-TMT (EC_{50} = 10 μM) compared to those for other tryptamines. We conducted a thorough pharmacological analysis of bufotenine derivatives to evaluate their hallucinogenic potential via 5-HT_{2A}R activation, comparing their receptor binding profiles and functional activities at 5-HT_{1A}R and 5-HT_{2A}R subtypes. 5-MeO-DMT demonstrates markedly greater potency at 5-HT_{2A}R (EC_{50} = 0.01 μM) compared to 5-OH-DMT (EC_{50} = 1 μM), being 100 times more potent. 5-OH-TMT showed a similar attraction to 5-HT_{1A}Rs (EC_{50} = 10 μM). The efficacy of 5-HT_{1A}R was greater for these compounds compared to that of 5-HT_{2A}R. Bufotenine derivatives generally showed greater potency for 5-HT_{1A}R than for 5-HT_{2A}R. The functional profile of 5-MeO-DMT closely aligns with the recently reported structural findings [37], with an approximately 10-fold difference in EC_{50} values, a variation that remains within an acceptable and interpretable range. In our experiments, bufotenine derivatives acted as full agonists in 5-HT_{1A}-mediated G-protein signaling compared to serotonin, despite variations in selectivity and potency. These findings validate the potency and efficacy of 5-MeO-DMT at 5-HT_{1A}, corroborating previous research highlighting the importance of 5-HT_{1A} in vivo pharmacology [38,39]. Our research demonstrates that 5-OH-DMT

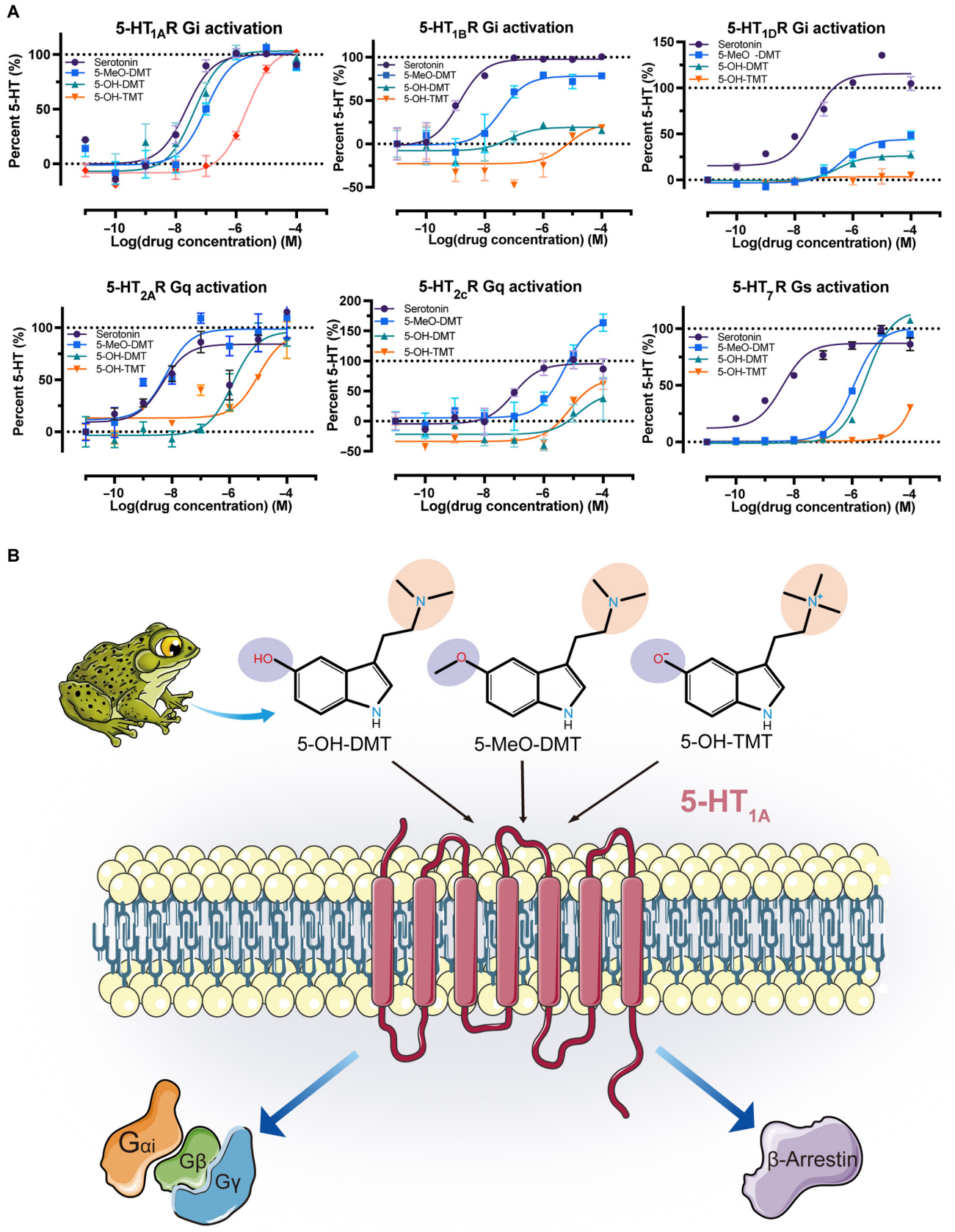


Fig. 1. Bufotenine derivatives acting at 6 depression-related serotonin receptors. (A) The difference of bufotenine derivative in activating depression-related serotonin receptors. (B) Schematic illustration of G-protein coupling of 5-HT_{1A} activated by a bufotenine derivative. 5-HT, serotonin; 5-HT_{1A}R, 5-HT_{1A} receptor; 5-HT_{1B}R, 5-HT_{1B} receptor; 5-HT_{1D}R, 5-HT_{1D} receptor; 5-HT_{2A}R, 5-HT_{2A} receptor; 5-HT_{2C}R, 5-HT_{2C} receptor; 5-HT_7R, 5-HT_7 receptor; 5-MeO-DMT, 5-methoxy-*N*,*N*-dimethyltryptamine; 5-OH-DMT, 5-hydroxy-*N*,*N*-dimethyltryptamine; 5-OH-TMT, 5-hydroxy-*N*,*N*,*N*-dimethyltryptamine.

exhibits greater efficacy as a 5-HT_{1A} agonist compared to 5-MeO-DMT and 5-OH-TMT, with 5-OH-TMT being the least potent.

Structures of bufotenine-derivative-bound 5-HT_{1A}

We generated 5-HT receptor–Gi complexes by coexpressing the receptors with a dominant-negative variant of human Gαi1 [40] and human Gβγ. The 5-HT_{1A}–Gi complexes coupled to 5-OH-TMT, 5-MeO-DMT, or 5-OH-DMT were analyzed, and their structures were determined at a resolution of 2.6 to 2.9 Å. The 5-MeO-DMT-bound 5-HT_{1A}–Gi complex and the 5-OH-DMT-bound HT_{1A}–Gi complex structures were resolved at a 2.9-Å resolution. The cryo-electron microscopy (cryo-EM) maps offer sufficient clarity to accurately identify the positions of the receptor, G-protein trimer, and bound ligands within the receptor–G-protein complexes (Fig. 2A to C, Figs. S1 to S4, and Table S1). Our structure shows a high degree of similarity to the recently reported 5-MeO-DMT–5-HT_{1A} complex, with only minor differences (Fig. S6F) [37]. The cryo-EM maps of 5-HT_{1A} with 5-OH-TMT, 5-MeO-DMT, and 5-OH-DMT show unique structures that align precisely with a phosphatidylinositol-4-phosphate (PtdIns4P) molecule [41]. Our previous research demonstrated that PtdIns4P acts as a positive allosteric modulator

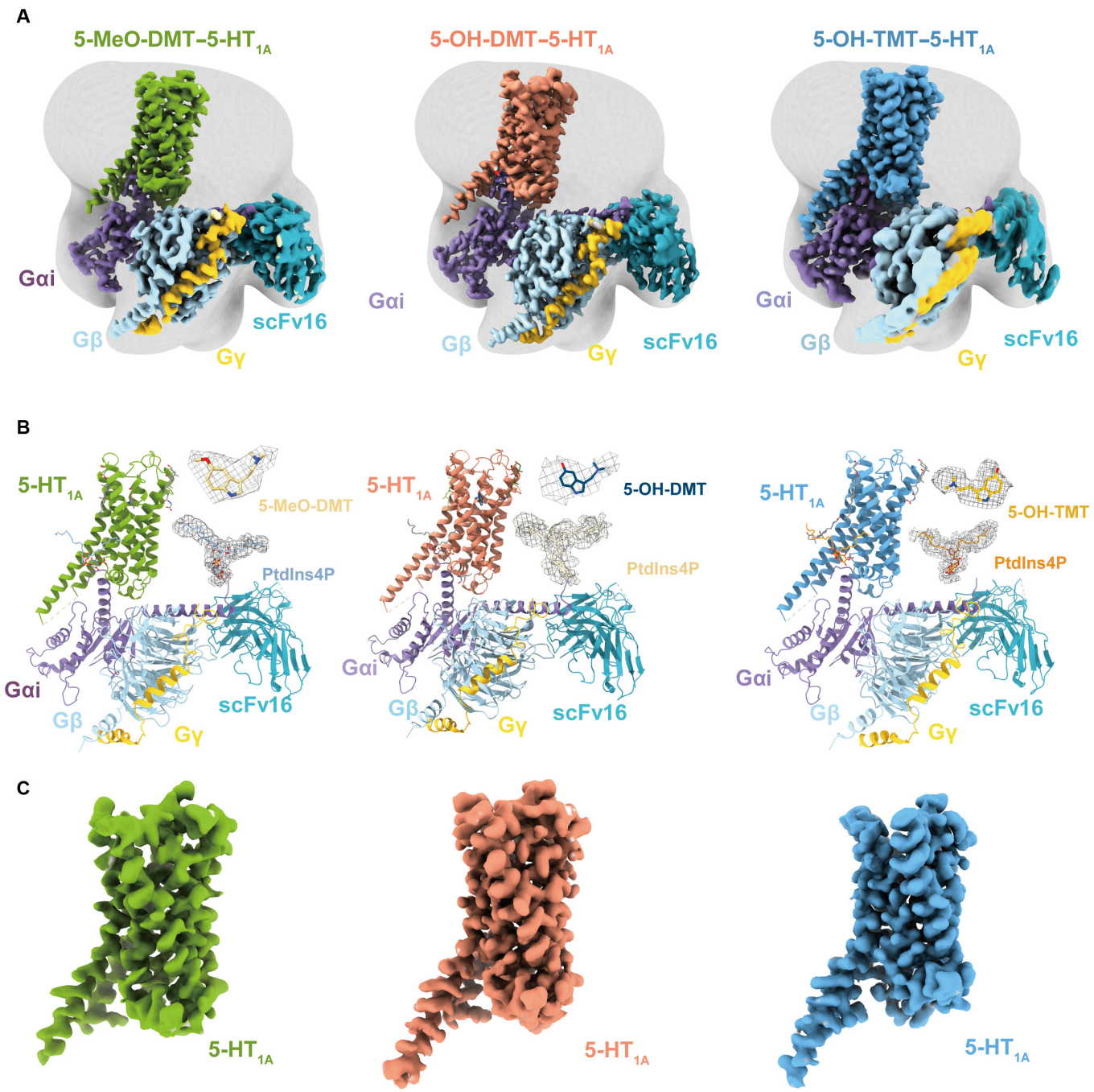


Fig. 2. Cryo-electron microscopy (cryo-EM) structures of 5-MeO-DMT–5-HT_{1A}–Gi–scFv16, 5-OH-DMT–5-HT_{1A}–Gi–scFv16, and 5-OH-TMT–5-HT_{1A}–Gi–scFv16 complexes. (A to C) Cryo-EM density maps (A and C) and cartoon representation (B) of 5-MeO-DMT–5-HT_{1A}–Gi–scFv16, 5-OH-DMT–5-HT_{1A}–Gi–scFv16, and 5-OH-TMT–5-HT_{1A}–Gi–scFv16. Composite DeepEMhancer sharpened cryo-EM density maps colored by protein components. PtdIns4P, phosphatidylinositol-4-phosphate.

of 5-HT$_{1A}$ by enhancing its basal activity and facilitating Gi recruitment and that 5-HT$_{1A}$ is further surrounded by diverse lipid species at the membrane interface [41].

Binding mode of bufotenine derivatives at 5-HT$_{1A}$

The structures we have discovered demonstrate distinct interactions between drugs and receptors within the orthosteric binding pocket (OBP), perhaps resulting in variations in pharmacological effects. The binding position of bufotenine derivatives in 5-HT$_{1A}$R complexes closely resembles that of serotonin within the receptor's structure (Fig. 3A and B). Bufotenine derivatives binding to the orthosteric pocket of 5-HT$_{1A}$ complexes apply downward pressure on the toggle switch residue W358$^{6.48}$ (Fig. S5A), leading to conformational changes in F354$^{6.44}$ and I124$^{3.40}$ within the PIF motif (Fig. S5B) and R134$^{3.50}$ in the DRY motif (Fig. S5C). Conformational changes disrupt the conserved ionic lock between TM3 and TM6, leading to a notable outward shift of TM6 by approximately 13.7 Å

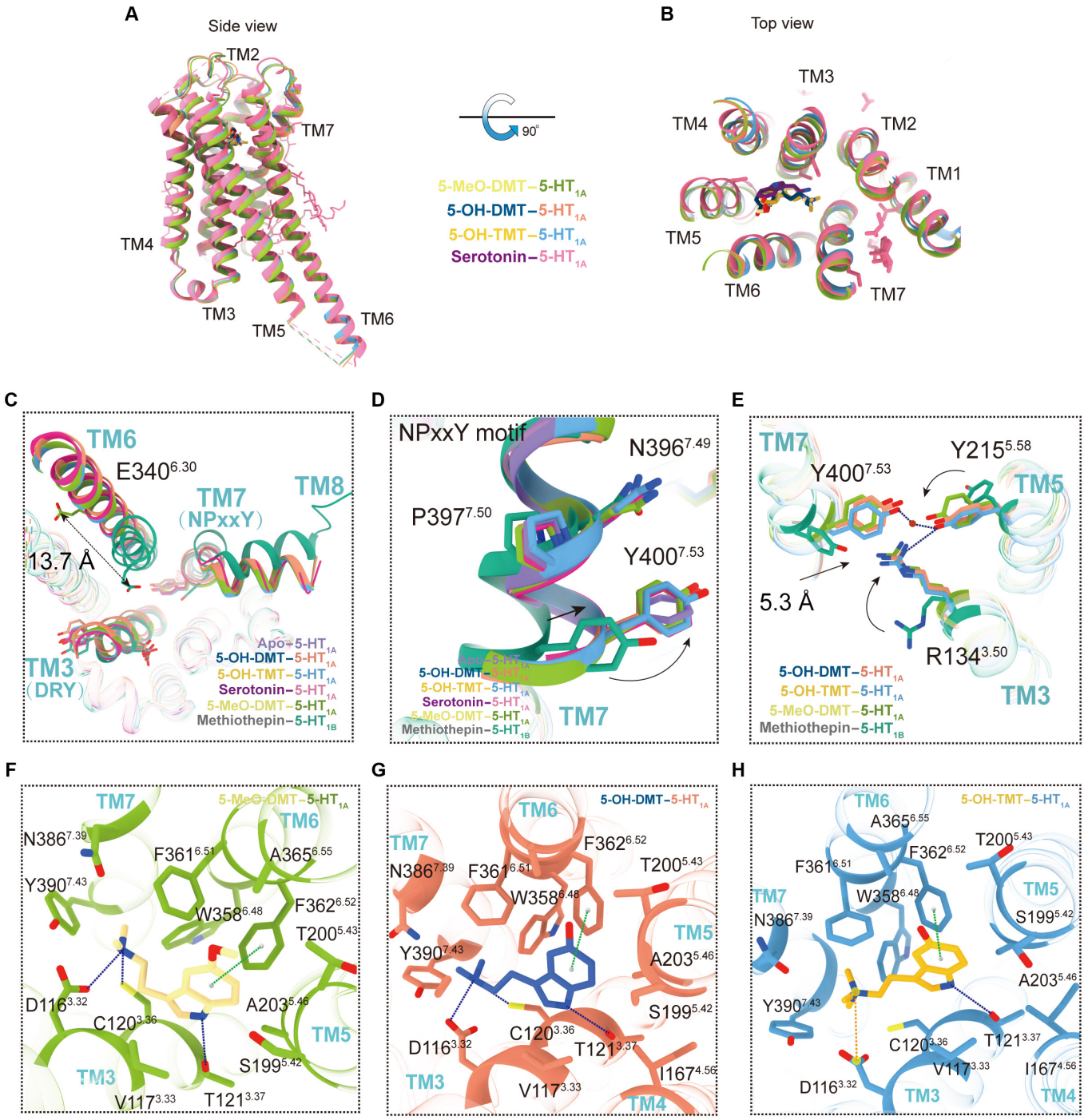


Fig. 3. Structural features of 5-HT$_{1A}$ in the active state by bufotenine derivatives. (A and B) Structural superposition of bufotenine-derivative-bound 5-HT$_{1A}$ and 5-HT-bound 5-HT$_{1A}$, presented from both the side view (left) and top view (right). (C to E) Conformational changes of the conserved "microswitches" upon receptor activation. The outward movement of the TM7 of the active receptor and the conformational changes of residue side chains are highlighted as black arrows. (F to H) Polar interaction network that stabilizes the conformation of bufotenine-derivative-bound 5-HT$_{1A}$, respectively (dotted blue line, hydrogen bonds; ochre brown, salt bridges; dotted green line, $\pi-\pi$ interactions).

at the Cα of E340$^{6.30}$ at the cytoplasmic end of TM6 (Fig. 3C). The inward shift of approximately 5.3 Å at the cytoplasmic end of TM7 enables hydrogen bonding between the Y400$^{7.53}$ of the NPxxY motif and Y215$^{5.58}$ with the R134$^{3.50}$ of the DRY motif (Fig. 3D and E). These conformational alterations facilitate the accessibility of the receptor's cytoplasmic pocket for Gi binding.

The identification of bufotenine derivatives relies on 2 key chemical elements: the indole ring and the ethylamine side chain (Fig. S6A to C), which mostly occupy the OBP. The indole ring serves as the fundamental structure of bufotenine derivatives. The indole ring primarily participates in π–π interactions with F361$^{6.51}$ and F362$^{6.52}$, as Ballesteros–Weinstein numbering (Fig. 3F to H) [42]. In the lower region of the 5-HT$_{1A}$ binding pocket, the indole nitrogen of bufotenine derivatives establishes a hydrogen bond with T121$^{3.37}$ (Fig. 3F to H), causing a 16.0° to 39.3° angle rotation of the bufotenine derivatives around the axis of the indole nitrogen (Fig. S6D).

Bufotenine derivatives are primarily distinguished by the position of the indole ring, specifically at the 3 and 5 locations, with an ethylamine side chain attached to the 3 position (Fig. S6A to C). This side chain imparts tryptamine characteristics to the bufotenine derivatives. The indole ring has a hydroxyl group at the 5-position. This property also differentiates the bufotenine derivatives from one another (Fig. S6A to C). Furthermore, the indole ring of 5-OH-DMT establishes a hydrophobic contact with I189^{ECL2} located in extracellular loop 2 of 5-HT$_{1A}$R (Fig. S6E). This is a notable distinction among the 3 derivatives that is not observed in the other 2 compounds. Both 5-OH-DMT and 5-OH-TMT were observed to have the indole ring interacting with I167$^{4.56}$; however, this interaction was not observed in 5-MeO-DMT (Fig. 3F to H). Additionally, the indole ring forms notable interactions with adjacent residues within the pocket, including V117$^{3.33}$, S199$^{5.42}$, T200$^{5.43}$, A203$^{5.46}$, and A365$^{6.51}$ (Fig. 3F to H and Fig. S7). The ethylamine side chain has the ability to establish a hydrogen bond with the nearby D116$^{3.32}$, which results in a certain alignment of the bufotenine derivatives (Fig. 3F to H). The positive charge on the ethylamine side chain of 5-OH-TMT prevents additional hydrogen bonding with adjacent nitrogen atoms. Nevertheless, this favorable charge also promotes the stability of the ligand within the pocket by salt bridge interactions (Fig. 3H). The ethylamine side chain interacts with the receptor via residues C120$^{3.36}$, W358$^{6.48}$, N386$^{7.39}$, and Y390$^{7.43}$ (Fig. S6E). In general, the alterations made to the ligand do not change the way it binds. Similar to the binding mechanism of serotonin, we discovered that the sites D116$^{3.32}$ and T121$^{3.37}$ were crucial in the binding of bufotenine derivatives to 5-HT$_{1A}$ (Fig. S6E). Following the mutation of the D116$^{3.32}$ and T121$^{3.37}$ sites to alanine, EC_{50} decreased by around 100-fold.

Through the alanine mutants of F361$^{6.51}$ and W358$^{6.48}$, we discovered a significant decrease in the potency of the 3 bufotenine derivatives in activating 5-HT$_{1A}$R (Fig. S7 and Table S2). F361$^{6.51}$ stabilizes the tryptamine scaffold's structure and is essential for the efficacy of different amine replacements. Previous studies have shown that A361$^{6.51}$, located adjacent to the 4-indole and 5-indole substituents in the 5-HT receptor, is specifically linked to 5-HT$_{1A}$R and is essential for determining its ligand selectivity (Fig. 2G to I and Fig. S7B, E, and H). In order to examine the underlying mechanism of ligand selectivity, we introduced a mutation at position A365$^{6.55}$, replacing it with phenylalanine. We detected a reduction in the potency of all analyzed tryptamine derivatives, with 5-OH-DMT exhibiting the most significant loss in potency, estimated to be around 1,000-fold less potent (Fig. S7E). Therefore, the presence of A365$^{6.55}$ in 5-HT$_{1A}$R is crucial for the strong effectiveness of 5-substituted tryptamines. This may be because A365$^{6.55}$ has the capacity to accept groups with diverse chemical characteristics.

Structural insights from bufotenine-derivative-bound 5-HT$_{2A}$R

To investigate the variations in the strength of bufotenine derivatives at 5-HT$_{1A}$R and 5-HT$_{2A}$R, we employed molecular docking to forecast the arrangement of bufotenine derivatives binding with 5-HT$_{2A}$ (PDB: 7RAN). In comparison to 5-HT$_{2A}$R, 5-HT$_{1A}$R exhibited an outward displacement of about 8.1 Å in the TM6 region, whereas TM8 was elevated by almost 2 Å (Fig. 4A). This change may be associated with the binding of PtdIns4P between TM6 and TM7. It is important to mention that 5-MeO-DMT has greater interactions with the V235$^{5.39}$ and F234$^{5.38}$ residues on TM5 in 5-HT$_{2A}$. This, together with the influence of L229^{ECL2}, causes a shift of about 1.89 Å toward TM5 (Fig. 4B). The structural analysis of 5-OH-DMT–5-HT$_{2A}$ reveals that the I163$^{3.40}$ residue on TM3 and the V235$^{5.39}$ residue on TM5 interact with the ligand (Fig. 4C). Unfortunately, the I167$^{4.56}$ residue site is absent on TM4. Furthermore, the indole ring of the ligand linked to 5-HT$_{2A}$ undergoes a 25° upward rotation when N343$^{6.55}$ replaces A365$^{6.55}$ on 5-HT$_{1A}$ TM6 (Fig. 4D). These circumstances may cause a significant drop in potency and reduced efficacy with 5-HT$_{2A}$, roughly 10 times lower than normal (Fig. 1A). The occurrence of 5-OH-TMT in 5-HT$_{2A}$ results in a displacement of about 1.18 Å toward TM5. This displacement might be attributed to the lack of I167$^{4.56}$ on TM4 and the presence of V235$^{5.39}$ on TM5 (Fig. 4E). Mutation data also demonstrated that 5-OH-TMT exhibited no alteration in affinity for both receptors but displayed a small increase in activity specifically toward 5-HT$_{1A}$. In the structural comparison, the indole ring of bufotenine derivatives in 5-HT$_{1A}$ is rotated about 26.6° relative to 5-HT$_{2A}$, altering the local polarity effect (Fig. 4F).

Structures of therapeutic drugs bound to 5-HT$_{1A}$

5-HT$_{1A}$ serves as a therapeutic target for the anxiolytic medication buspirone and the antidepressant vilazodone, both of which are often utilized in clinical practice. In the comparison of commonly used clinical drugs, we conducted functional experiments. The findings indicated that the EC_{50} values of 2 buprenorphine derivatives were approximately comparable to those of clinically utilized drugs (Fig. 5A). All 6 compounds reside in the OBP; however, they exhibit varying depths and an extended binding pocket (PDB: 7E2Z, 8FYL, and 8FYX) (Fig. 5B). Buspirone had the highest potency, with an EC_{50} of 1 nM. 5-MeO-DMT, 5-OH-DMT, aripiprazole, and vilazodone exhibited comparable affinities, with EC_{50} spanning around 10 to 100 nM. Unlike tryptamine derivatives, aripiprazole may interact with the N387$^{7.40}$ residue site on TM7, a unique binding site believed to stabilize the quinolone segment of aripiprazole inside the 5-HT$_{1A}$ extended binding pocket (Fig. 5C). The vilazodone molecule contains an indole core that is connected to the OBP. The W387$^{7.40}$ residue on TM7 and the Y96$^{2.64}$ residue on TM2 exhibit π–π interactions with the benzofurano-carboxamide group of vilapatone (Fig. 5D). Aripiprazole and exrazolone possess similar OBP structures, characterized by the inward rotation of the indole ring at W387$^{7.40}$ and the phenolic

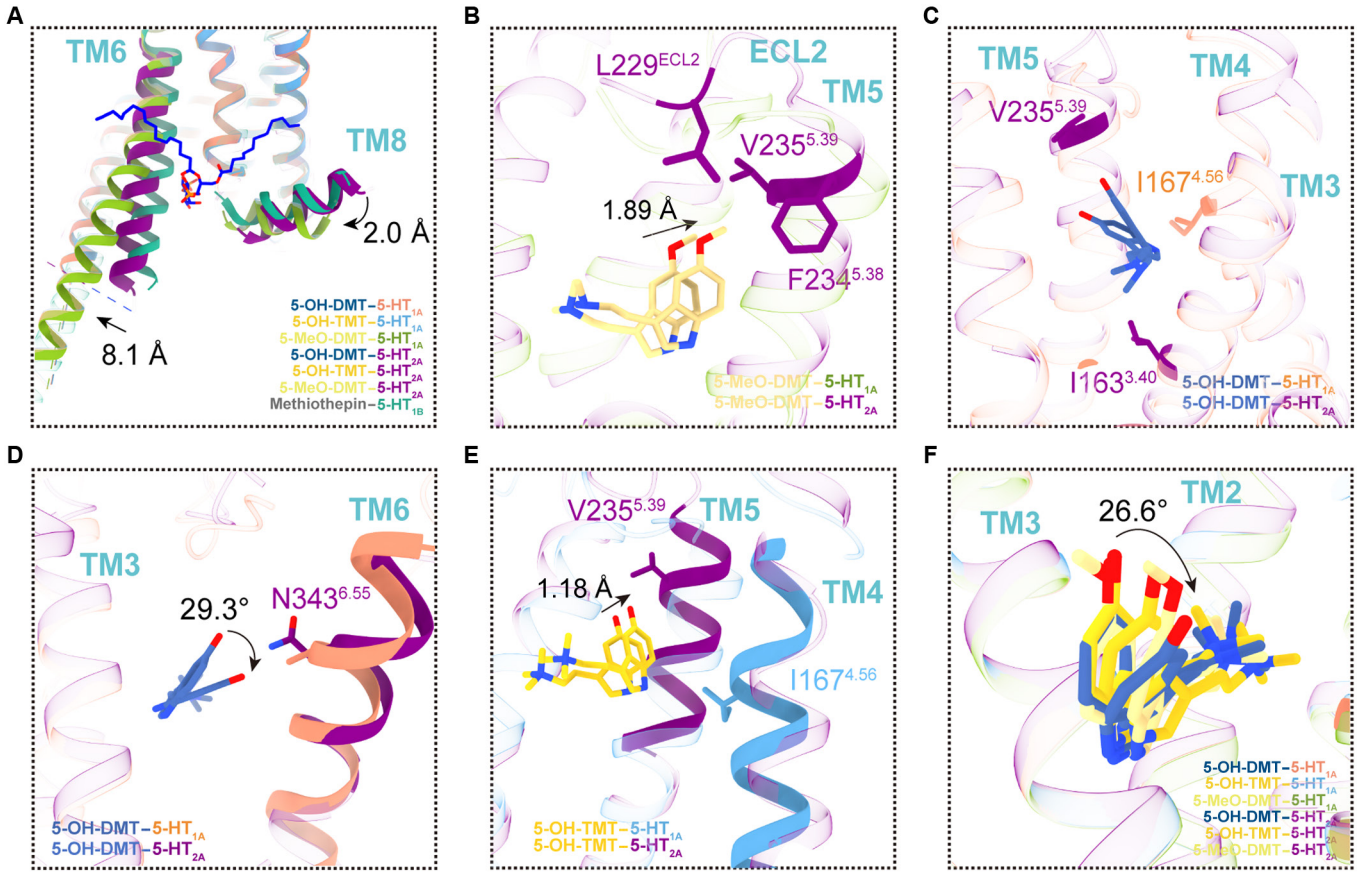


Fig. 4. Structural comparison of bufotenine derivatives in relation to 5-HT_{1A}R, 5-HT_{1B}R, and 5-HT_{2A}R. (A) 5-HT_{1A}R displaces TM6 and TM8 outward and downward during activation, attributed to PtdIns4P binding between TM6 and TM7. Aligned structures of the inactive-state 5-HT_{1B} (bound to the inverse agonist methiothepin; PDB: 6G79). (B) Unlike the 5-MeO-DMT–5-HT_{1A} structure, 5-MeO-DMT–5-HT_{2A} shifts the ligand toward TM5 during activation. (C and D) The 5-OH-DMT–5-HT_{1A} structure experiences rotation of the indole ring during activation. (E) The ligand is shown to migrate toward TM5 in the 5-OH-TMT–5-HT_{2A} structure. (F) In contrast to 5-HT_{2A}, the indole ring of bufotenine derivatives in 5-HT_{1A} is rotated, modifying the local polarity effect. The black arrows indicate the trajectory of the receptor helix or the residues' side chain's migration.

hydroxyl group at $Y96^{2.64}$, hence augmenting polar contacts, in stark contrast to the tryptamine derivatives. The benzofurancarboxamide moiety of vilazodone extends toward the extracellular site, whereas the piperazine part is positioned closer to the extracellular area compared to other compounds. The presence of this characteristic may be attributed to the distinct binding configurations of vilazodone and aripiprazole. In particular, the *N*-aryl substituent of aripiprazole and the *N*-alkyl substituent of vilazodone attach to the OBP, causing $D116^{3.32}$ and $Y390^{7.43}$ to interact with the identical piperazine in both drugs (Fig. 5E). The prolonged pocket in the structure of buspirone is maintained by the involvement of $M92^{2.60}$, $A93^{2.61}$, and $C187^{ECL2}$ at the TM2 location. Buspirone has a distorted structural conformation, whereby the azacyclodecane-7,9-dione component curves into the interstice between TM2 and TM3, causing the side chains of $M92^{2.60}$ and $F112^{3.28}$ to rotate outward accordingly (Fig. 5F). Within the context of the OBP, the piperazine component of buspirone engages with $D116^{3.32}$ in a way akin to aripiprazole (Fig. S5D). Specifically, the pyrimidine portion of buspirone is positioned in close proximity to TM3 and TM5, resulting in mostly hydrophobic interactions (Fig. S5E). In general, we see that although they have distinct structures, vilazodone, aripiprazole, and buspirone have comparable orientations in the central binding pocket. The aromatic piperazine substituents of these compounds are mostly stabilized by phenylalanine residues in TM6 ($F361^{6.51}$ and $F362^{6.52}$) (Fig. S5F). Therefore, it may be inferred that bufotenine derivatives have pharmacological actions that are comparable to those of antidepressants, as they display a similar binding pattern in the OBP.

5-OH-DMT and 5-MeO-DMT exhibited similar improvement against depressive-like behaviors through 5-HT_{1A}R

We explored the therapeutic effects of 5-MeO-DMT and 5-OH-DMT on depression and the involvement of 5-HT_{1A}R by stereotactically injecting AAV with Syn-eGFP-sh-5-HT_{1A}R to knock down 5-HT_{1A}R in the hippocampus (Figs. S8 and S9). Here, we focused on 5-HT_{1A}R in the mouse hippocampus, because the hippocampus is of particular importance in regulating mood and adult neurogenesis, as well as the highest levels of 5-HT_{1A}R in the hippocampal area [43–45]. Mice were subjected to chronic unpredictable mild stress (CUMS) to model depression, and their condition was assessed through behavioral tests (Fig. S8A). CUMS prolongs immobility periods in both negative control (NC) and sh-5-HT_{1A}R mice during the tail suspension test (TST) and forced swimming test (FST). In NC mice, 5-MeO-DMT and 5-OH-DMT significantly reduce immobility time in both TST (5-MeO-DMT: 80.21%;

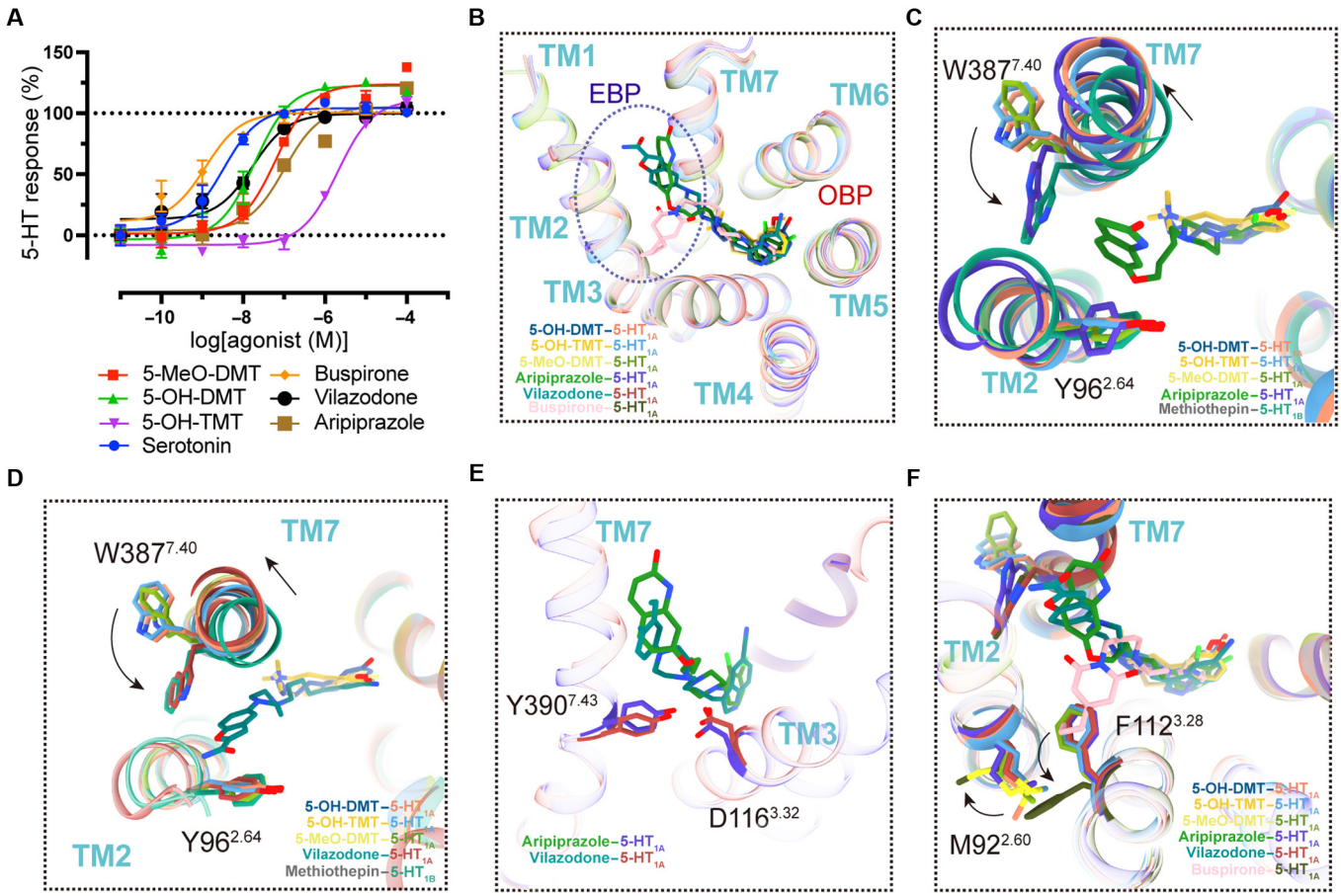


Fig. 5. Structural and functional comparison of bufotenine derivatives and clinical 5-HT$_{1A}$ medications at 5-HT$_{1A}$. (A) 5-HT$_{1A}$–Gi GloSensor assays of 5-HT, 5-MeO-DMT, 5-OH-DMT, 5-OH-TMT, vilazodone, aripiprazole, and buspirone. All signaling experiments were performed in triplicate and were averaged from 3 independent experiments. Data were normalized against 5-HT, and errors bars denote the standard error of the mean (SEM). (B) Comparison of the positioning of bufotenine derivatives and therapeutic 5-HT$_{1A}$ medications inside the 5-HT$_{1A}$R pocket. (C) The quinolone segment of aripiprazole influences alterations in the side chain of the N387$^{7.40}$ residue and the displacement of TM7 inside the 5-HT$_{1A}$ extended binding pocket. (D) Vilapatone's benzofuranocarboxamide group affects the displacement of TM7 inside the 5-HT$_{1A}$ extended binding pocket as well as changes to the side chain of the N387$^{7.40}$ residue. (E) The *N*-aryl substituent of aripiprazole and the *N*-alkyl substituent of vilazodone attach to the orthosteric binding pocket (OBP). (F) The azacyclodecane-7,9-dione component of buspirone curves into the interstice between TM2 and TM3. The black arrows indicate the trajectory of the receptor helix or the residues side chain's migration. EBP, extended binding pocket.

5-OH-DMT: 83.06%) and FST (5-MeO-DMT: 31.03%; 5-OH-DMT: 54.46%). However, in sh-5-HT$_{1A}$R mice, the effects are diminished, with 5-MeO-DMT showing 77.37% efficiency in TST and 37.07% in FST and 5-OH-DMT showing 68.76% efficiency in TST and 46.50% in FST (Fig. 6A and B and Table S3). In the sucrose preference test, both 5-MeO-DMT and 5-OH-DMT significantly counteract the reduction in sucrose preference induced by CUMS. However, in comparison to NC mice, only sh-5-HT$_{1A}$R mice treated with 5-MeO-DMT show a decrease in sucrose preference (Fig. 6C and Table S3). The open-field test was conducted to assess anxiety-like behaviors. Results indicated that both 5-MeO-DMT and 5-OH-DMT increased the total distance traveled and time spent in the center, regardless of 5-HT$_{1A}$R knockdown. However, 5-MeO-DMT reduced total distance after 5-HT$_{1A}$R was knocked down (Fig. 6D and Table S3). Spatial learning and memory were assessed using the Morris water maze test. In NC and sh-5-HT$_{1A}$R mice, 5-MeO-DMT and 5-OH-DMT decrease escape latencies (5-MeO-DMT: 124.47% efficiency; 5-OH-DMT: 146.30% efficiency) and increase target crossing times (5-MeO-DMT: 76.47% efficiency; 5-OH-DMT: 111.76% efficiency). sh-5-HT$_{1A}$R mouse treatment with these 2 bufotenine derivatives increases escape latencies (efficiency of 5-MeO-DMT: 81.41%; efficiency of 5-OH-DMT: 81.93%), but only 5-OH-DMT reduces times across target (efficiency: 110.00%), compared to NC mice (Fig. 6E and Table S3). The findings indicate that both 5-MeO-DMT and 5-OH-DMT similarly alleviate CUMS-induced depressive-like and anxiety-like behaviors, as well as enhance learning and memory via 5-HT$_{1A}$R. Furthermore, it is worth noting that in contrast to 5-MeO-DMT, 5-OH-DMT treatment resulted in somewhat reduced head-twitch response (HTR) and incremental horizontal locomotor activity (HLA) in mice (Fig. S10), indicating diminished hallucinogenic potential while preserving therapeutic antidepressant effects.

To further validate that 5-OH-DMT elicits antidepressant-like action via 5-HT-dependent mechanism, we generated a 4-chloro-DL-phenylalanine (PCPA)-induced mouse model of depression and anxiety and gave treatment with or without 5-OH-DMT (15 mg/kg) and 5-HT$_{1A}$R antagonist WAY100635 before behavioral tests (Fig. S8B). As expected, compared with the control or model group, WAY100635 significantly increased immobility time in both TST and FST. In comparison, mice treated with 5-OH-DMT exhibited shorter immobility durations in these tests. However, the addition of WAY100635 to

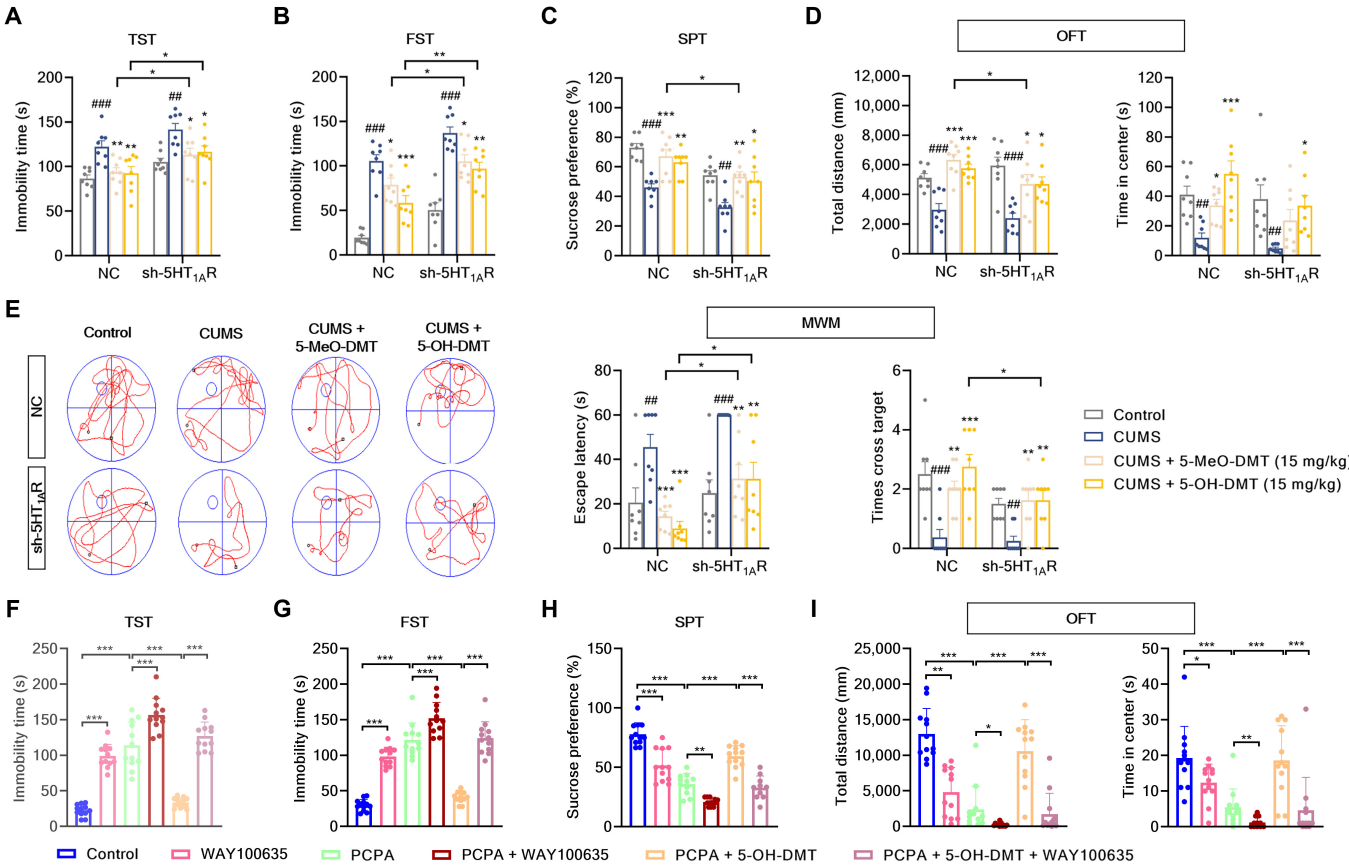


Fig. 6. 5-OH-DMT and 5-MeO-DMT exhibited similar improvement against depressive-like behaviors through 5-HT_{1A}R. The (A) tail suspension test (TST), (B) forced swimming test (FST), (C) sucrose preference test (SPT), (D) open-field test (OFT), and (E) Morris water maze test (MWM) were performed in negative control (NC) and sh-5-HT_{1A}R mice treated with or without chronic unpredictable mild stress (CUMS), 5-MeO-DMT, and 5-OH-DMT ($n = 8$). (F) TST, (G) FST, (H) SPT, and (I) OFT were performed in mice treated with or without 4-chloro-DL-phenylalanine (PCPA), 5-OH-DMT, and the 5-HT_{1A}R antagonist WAY100635 ($n = 12$). All quantification data are presented as mean ± SEM. $^{\#}P < 0.05$ and $^{\#\#}P < 0.001$ versus the control group; $^{*}P < 0.05$, $^{**}P < 0.01$, and $^{***}P < 0.001$ versus the model group.

the PCPA and 5-OH-DMT group also prolonged the immobility time in both TST and FST (Fig. 6F and G). WAY100635 reduced sucrose preference compared to the control or model group. Conversely, treatment with 5-OH-DMT increased sucrose preference in mice, while this increase was reversed by WAY100635 (Fig. 6H). In addition, mice treated with WAY100635 showed less total distance traveled and less time spent in center compared to the control or PCPA mice in the open-field test. By contrast, 5-OH-DMT dramatically increased both the total distance and time spent in the center, whereas the administration of WAY100635 in the PCPA and 5-OH-DMT group significantly recovered these changes (Fig. 6I). These results reconfirmed that 5-OH-DMT ameliorates depressive-like behaviors through 5-HT_{1A}R.

Discussion

The role of 5-HT_{1A}R signaling in the therapeutic efficacy of antidepressants is well established [46–48]. Here, we provide the molecular structures of bufotenine derivatives in complex with 5-HT_{1A}R, alongside a comprehensive analysis of their signaling behaviors at this receptor. This approach illuminates the precise relationship between the chemical configurations of bufotenine derivatives and their functional effects. Notably, bufotenine derivatives exhibit a more inclined orientation within the binding pocket compared to serotonin, with structural differences across binding sites influencing their interaction profiles. The structure–activity relationships reveal distinct contributions of key functional groups to 5-HT_{1A}R binding and activation. The hydroxyl group at the 5-position of the indole ring serves as a critical hydrogen bond donor, potentially interacting with polar residues such as $D116^{3.32}$ or $S199^{5.42}$ within the OBP, thereby enhancing binding affinity and stabilizing the ligand–receptor complex [49–51]. This hydroxyl substitution distinguishes bufotenine derivatives from other tryptamines and may account for their unique pharmacological profile. Methoxy substitutions introduce additional steric bulk and electron-donating properties that can modulate receptor selectivity [52–54]. The methoxy group's oxygen atom may participate in weak hydrogen bonding interactions with backbone amides or hydroxyl-containing residues, while its methyl component influences overall lipophilicity and membrane permeability [55]. Importantly, methoxy groups at different positions (e.g., 4-methoxy vs. 7-methoxy) create distinct binding orientations within the pocket, potentially explaining subtype selectivity between 5-HT_{1A} and other serotonin receptors [37,56]. *N*,*N*-Dimethyl substitutions on the ethylamine side chain significantly impact both binding kinetics and efficacy. The methyl groups increase the basicity of the amine nitrogen, enhancing ionic interactions with the conserved $D116^{3.32}$ that anchors most aminergic ligands. Additionally, the steric hindrance imposed by N-methylation may restrict conformational flexibility, favoring specific receptor conformations

associated with particular signaling pathways. This could explain why certain *N*-methyl derivatives show biased signaling toward G-protein activation over β-arrestin recruitment, contributing to their therapeutic potential with reduced side effects [57]. These variations in structure modulate the activity and affinity of bufotenine derivatives at 5-HT_{1A}R and 5-HT_{2A}R.

We speculate that 5-OH-DMT's unique hydrogen bonding with $I189^{ECL2}$ reduces β-arrestin recruitment, which may be associated with its low hallucination risk; however, this mechanistic explanation requires further validation through in-depth studies of receptor trafficking dynamics and electrophysiological consequences. Fluorescence recovery after photobleaching studies could quantify 5-HT_{2A}R internalization rates and recycling kinetics following 5-OH-DMT treatment compared to classical hallucinogens. Additionally, whole-cell patch-clamp recordings in cortical pyramidal neurons would reveal the temporal profile of receptor activation and downstream effector coupling. Brain slice electrophysiology could assess network-level effects, particularly examining gamma oscillations in layer 2/3 cortical circuits that correlate with hallucinogenic experiences. Such studies would provide mechanistic validation of our molecular findings and establish the functional significance of reduced β-arrestin signaling. Furthermore, 2-photon calcium imaging in awake behaving animals could bridge molecular mechanisms with behavioral phenotypes, ultimately supporting the therapeutic potential of 5-OH-DMT derivatives.

Importantly, bufotenine derivatives display unique conformations and distinct structural attributes relative to traditional antidepressants, enabling the development of structure-based bufotenine derivatives with selective 5-HT_{1A}R activity and reduced affinity for 5-HT_{2A}Rs. Given that hallucinogenic effects are predominantly associated with 5-HT_{2A}R activation, the comparatively moderate hallucinogenic potential of 5-HT_{1A}R is notable. Since 5-MeO-DMT clearly targets 5-HT_{2A}R, we focused on 5-OH-DMT in our in vivo experiments. Bufotenine derivatives demonstrate a significant enhancement in antidepressant efficacy in the CUMS model or PCPA model. Knockdown of hippocampal 5-HT_{1A}R partly abolishes the effect of 5-OH-DMT in improving CUMS-induced depressive-like behaviors. However, the 5-HT_{1A}R antagonist WAY100635 almost completely abolishes the antidepressant effect of 5-OH-DMT in the PCPA model. These differential effects might be explained by that except for the hippocampus, other brain regions also participate in 5-OH-DMT-exerted antidepressant effect. Moreover, PCPA-induced depression is clearly due to serotonin depletion, while the mechanism of CUMS-induced depression is more complex. Our findings confirm bufotenine derivatives as full agonists at 5-HT_{1A}R. These insights underscore the potential of bufotenine derivatives as a promising avenue for targeted antidepressant development. Further study is needed to test 5-HT_{1A} agonists such as buspirone or vilazodone in biological experiments to support any competitive advantage for bufotenine derivatives.

Psychedelics are increasingly recognized as potential treatments for neuropsychiatric disorders. Classical psychedelics primarily target 5-HT_{2A}R on cortical pyramidal neurons, influencing their hallucinogenic and subjective effects [58]. However, whether 5-HT_{2A}R activation is indispensable for the neuroplastic and therapeutic potential of psychedelics remains debated. Growing evidence suggests that psychedelics exhibit complex polypharmacological profiles that extend beyond their 5-HT_{2A}R-mediated hallucinatory actions. Receptors like TrkB, 5-HT_{2C}, and 5-HT_{1A} are increasingly acknowledged as crucial binding sites that enhance the plasticity and therapeutic effectiveness of psychedelics, separate from their hallucinogenic effects [59]. 5-HT_{1A}R is implicated in the behavioral effects of tryptamine hallucinogens, especially 5-MeO-DMT, aligning with some findings from our study [37]. Psychedelics are thus likely to act through multiple pathways, with the specific receptor profiles engaged by each compound potentially optimizing their therapeutic utility across various disorders. Our findings demonstrate that bufotenine derivatives exert antidepressant effects primarily through 5-HT_{1A}R.

A diverse array of chemically distinct compounds is essential for developing new drugs targeting 5-HT_{1A}R, with tailored efficacy, activity, and selectivity profiles. Each psychedelic compound can elicit unique introspective effects, shaped by genetic differences that influence drug metabolism and individual responses. Although psychedelics often act on multiple molecular targets, their specific effects vary with chemical structure. Thus, identifying the optimal psychedelic-inspired treatment for a given condition is not always straightforward. Expanding the chemical landscape by considering both the subjective effects and structural diversity of these compounds is crucial for advancing personalized therapeutics.

Conclusion

In conclusion, our integrated structural and functional analyses reveal how bufotenine derivatives—5-MeO-DMT, 5-OH-DMT, and 5-OH-TMT—selectively engage and activate 5-HT_{1A}R at high resolution. These compounds demonstrate robust antidepressant efficacy in vivo while exhibiting attenuated hallucinogenic properties, largely attributed to their specific modulation of 5-HT_{1A}-mediated G-protein signaling. Collectively, our findings establish a mechanistic framework for the rational design of 5-HT_{1A}-targeted therapeutics and support the potential of bufotenine derivatives as promising candidates for the development of safer and more effective antidepressant and anxiolytic drugs.

Methods

Creating compounds through chemical reactions

Compound 1 (5-MeO-DMT) was synthesized by reacting (4-methoxyphenyl)hydrazine hydrochloride (5.0 mmol) with 4,4-diethoxy-*N*,*N*-dimethyl-1-butylamine (5.25 mmol) in water and sulfuric acid under N_2 at 37 °C for 14 h. The mixture was basified (pH 10) and extracted with ethyl acetate. The crude product was purified via silica gel chromatography (dichloromethane [DCM]:methanol [MeOH] = 30:1) to yield a brown-yellow paste (684.4 mg, 62.7%). ^{1}H nuclear magnetic resonance (NMR) (500 MHz, $CDCl_3$) δ 7.94 (s, 1H), 7.24 (d, J = 8.8 Hz, 1H), 7.05 (d, J = 2.4 Hz, 1H), 7.00 (d, J = 2.4 Hz, 1H), 6.85 (dd, J = 8.8, 2.4 Hz, 1H), 3.86 (s, 3H), 2.93 to 2.88 (m, 2H), 2.65 to 2.61 (m, 2H), 2.34 (s, 6H). ^{13}C NMR (500 MHz, $CDCl_3$) δ 154.07, 131,56, 127.74, 122.58, 112.00, 100.67, 59.79, 56.00, 44.97, 23.21.

Compound 2 (5-OH-DMT) was prepared using 5-benzyloxyindole (10 mmol) and oxalyl chloride (20 mmol) in anhydrous diethyl ether at room temperature for 30 min. The red solid was collected by filtration, washed with ether, and dried under vacuum to afford 5-benzyloxy-3-indol-glyoxylylchloride. An aqueous NaOH solution was added dropwise to a suspension of 5-benzyloxy-3-indol-glyoxylylchloride (10 mmol) and

dimethylamine hydrochloride (42.9 mmol) in ether at 25 °C for over 30 min. The crude product was obtained by filtration. The product was hydrogenated (10% Pd/C, H_2, 24 h), filtered, and purified via silica gel (DCM:MeOH = 30:1) to give 6.1 g of the product (92% yield). The product (35 mg, 0.15 mmol) was reduced with $LiAlH_4$ (9 mmol) in tetrahydrofuran at 0 °C, refluxed for 4 h, and then stirred at 40 °C for 10 h. After NaOH quenching and workup, column chromatography (CH_2Cl_2:MeOH = 10:1) gave compound 2 (5-OH-DMT) as a yellow-brown oil (85% yield). ^{1}H NMR (dimethyl sulfoxide-d_6 [DMSO-d_6], 500 MHz) and ^{13}C NMR confirmed the structure [60].

Compound 3 (5-OH-TMT) was obtained by methylating compound 2 (20 mmol) with methyl iodide (120 mmol) in MeOH under nitrogen for 24 h, followed by silver chloride treatment to remove iodide. After extraction and chromatography (DCM:MeOH = 20:1), 3.4 g of the product was isolated (47.9% yield). ^{1}H NMR (DMSO-d_6, 500 MHz) and ^{13}C NMR supported successful quaternization [60].

Construction

To achieve insert cell expression, Synbio Technologies optimized the human wild-type 5-HT_{1A} gene codons. A thermally stable apocytochrome b562 RIL was inserted at the N-terminal of human 5-HT_{1A}R to boost receptor expression [61]. The proteins included affinity markers like the N-terminal Flag and His tags. It was shown that L125W alterations in 5-HT_{1A} improved thermal stability [62]. The Vazyme Biotech ClonExpress II One-Step Cloning Kit cloned 5-HT_{1A}R into pFastBac. The receptor's N terminus was 24 residues short. Dominant-negative human Gαi1 was produced with mutations S47N, G203A, A326S, and E245A using site-directed mutagenesis. Mutations increase the dominant-negative impact by destroying the βγ subunits' stabilizing salt bridge [40]. Cloned pFastBac vectors include human dominant-negative Gαi1 (DNGαi1), Gβ1, and Gγ2 genes. A modified pFastBac vector cloned scFv16. The vector's N-terminus includes the GP67 secretion signal peptide. While being built, insect cell expression vectors created these structures.

Cell culture and protein expression

At 27 °C, High Five insect cells (Hi5, Invitrogen) were grown in ESF 921 serum-free medium (Expression Systems). Agilent HEK 293T cells were cultured in Thermo Fisher's Dulbecco's modified Eagle medium (DMEM) with 10% fetal bovine serum (FBS). A room with regulated humidity, 5% CO_2, and 37 °C temperature housed the cultivation. The Bac-to-Bac Baculovirus Expression System from Thermo Fisher developed baculoviruses. Human genes 5-HT_{1A}, DNGαi1, Gβ1, Gγ2, and scFv16 were coexpressed in High Five cells using Expression Systems' baculovirus technique. Cell cultures were grown to 2 to 3 million cells/ml and evenly treated to 5 baculoviruses. After 48 h of infection, centrifuged cells were kept at −80 °C for examination.

Purification of protein complexes

Cryopreserved cells were lysed in buffer (20 mM Hepes pH 7.5, 100 mM NaCl, 10% glycerol, 10 mM $MgCl_2$, and 5 mM $CaCl_2$) with EDTA-free protease inhibitors. After Dounce homogenization, 5-HT_{1A}–Gi–scFv16 complexes were formed by adding 25 mU/ml apyrase and 100 μM ligand at room temperature for 1.5 h. Membranes were solubilized in 0.5% lauryl maltose neopentyl glycol and 0.1% cholesteryl hemisuccinate at 4 °C for 2 h and clarified by ultracentrifugation (30,000 rpm, 30 min). The supernatant was incubated with Talon beads for 2 h at 4 °C. After washing with low imidazole buffer, bound complexes were eluted with 250 mM imidazole. The eluate was concentrated using a 100-kDa cutoff filter and purified by size-exclusion chromatography (Superose 200 Increase 10/300 GL). Eluted fractions were analyzed by sodium dodecyl sulfate–polyacrylamide gel electrophoresis (Figs. S1 to S3). For cryo-EM investigation, receptor–Gi-protein complex samples were combined and condensed.

Cryo-EM data acquisition

Purified 5-MeO-DMT-, 5-OH-DMT-, and 5-OH-TMT-bound 5-HT_{1A}–Gi–scFv16 complexes (12, 10, and 13 mg/ml) were vitrified on glow-discharged Quantifoil grids using a Vitrobot at 4 °C. Cryo-EM data were acquired on a Titan Krios G4 (300 kV) with a Falcon 4i detector and Selectris X, collecting 13,026, 5,233, and 5,387 electron event representation (EER) movies at 0.73 Å/pixel, 10 $e^-/Å^2/s$, with defocus from −0.8 to −1.8 μm.

Image processing and 3-dimensional reconstruction

Motion correction was performed using MotionCor2 [63,64], and contrast transfer function estimation was done with CTFFIND [65] in cryoSPARC. Low-quality micrographs (>4.0 Å or carbon contaminated) were excluded. Particle picking (blob, Topaz, template) and 2-dimensional classification identified high-quality particles for ab initio reconstruction and heterogeneous refinement. After merging and de-duplication, 180,694, 195,003, and 139,905 particles were refined for the 5-MeO-DMT, 5-OH-DMT, and 5-OH-TMT complexes, respectively, yielding global resolutions of 2.63, 2.54, and 2.59 Å, respectively. Local refinement on the receptor achieved 2.75, 2.55, and 2.74 Å, respectively, followed by DeepEMhancer [66] post-processing (Figs. S1 to S3).

Model building and refinement

The density maps were fitted with structural models of 5-HT_{1A}, Gαi, Gβ, Gγ, and scFv16 from PDB entries 7E2Z and 7YS6 (Fig. S4) [41]. Initial fitting into locally refined receptor maps was performed in UCSF Chimera [67], followed by iterative manual adjustments in COOT [68] and automated refinement in PHENIX [69]. G protein and receptor models were further fitted into B-factor-sharpened maps, refined in COOT and PHENIX, and subjected to additional reconstruction using ISOLDE [70] and PHENIX with torsion restraints. Final models were validated via PHENIX cryo-EM validation (Table S1). Figures were prepared using Chimera, ChimeraX [71], and PyMOL (Schrödinger, LLC.).

Molecular docking

The molecular docking models were constructed using the 5-HT_{2A} structures (PDB: 7RAN). The models were generated by removing all ligands and water molecules from these structures. The PubChem database (https://pubchem.ncbi.nlm.nih.gov/) was used to download the structures of the small-molecule ligands of interest. At a physiological pH of 7.4 and using AMBER ff 14SB parameters [72], protonation states were assigned using H++ 3.2v (http://newbiophysics.cs.vt.edu/H++/). Then, the Chiron tool was used to decrease energy in the protein structure [73]. At the center of *X*: 130.464, *Y*: 116.935, and *Z*: 87.163, the grid box covers virtually all of the pocket residues; the 5-HT_{1A} ligand docking grid line was *X*: 16.833, *Y*: 12.877, and *Z*:

14.753 (Å). Using AutoDock Vina (version 1.1.2) [74], docking computations were carried out. The ChimeraX software was used to view the docked protein–ligand structures.

Animals

Adult C57BL/6 male mice (6 to 8 weeks) were purchased from QingLongShan (Nanjing, China). The mice were individually housed at 18 to 22 °C with water and food ad libitum and at a 12:12 h light cycle.

Ethics statement

All experiments involving animals were conducted according to ethical policies and procedures approved by the Animal Care and Use Committee of Nanjing University of Chinese Medicine (Nanjing, China) (Approval No. A220404).

Stereotactic injections

Adeno-associated viruses (AAVs) encoding AAV-Syn-eGFP-scramble shRNA (1.26×10^{13} viral genomes/ml) and AAV-Syn-eGFP-sh-5-HT_{1A}R (1.10×10^{13} viral genomes/ml) were generated by OBIO Technology (Shanghai, China). Mice received stereotactic injections into the hippocampal region at the following coordinates relative to the bregma: anterior/posterior, −2 mm; mediolateral, ±1.5 mm; and dorsoventral, −1.8 mm [75]. Animals were injected with either 500 nl of viruses into both hemispheres to breed hippocampus-specific 5-HT_{1A}R knockdown (sh-5-HT_{1A}R) mice and NC mice. After 3 weeks, the efficiency of postinfection was verified by enhanced green fluorescent protein (eGFP) fluorescence and relative 5-HT_{1A}R messenger RNA level. For messenger RNA detection, hippocampal RNA was isolated and first-strand complementary DNA was synthesized using HiScript II Q RT SuperMix. Quantitative real-time polymerase chain reaction (PCR) was performed with ChamQ SYBR qPCR Master Mix in CFX Connect Real-Time PCR Detection System (Bio-Rad, Redmond, USA). The primers used in this study were as follows: 5-HT_{1A}R F, CATCGCGCTAGACAGGTACTG; 5-HT_{1A}R R, CAATGAGCCAAGTGAGCGAGA; β-actin F, GTGACGTTGACATCCGTAAAGA; and β-actin R, GCCGGACTCATCGTACTCC.

CUMS model and treatment

Mice were divided into the control or CUMS model group. For the CUMS model group, mice were exposed to randomized stressors at least once a day over 5 weeks, including 24-h water/food deprivation, reversed light/dark cycle, 24-h soiled/empty cage, 24-h cage tilt, 5-h confinement, 5-min cold swimming, and 6-h noise (80 dB). The control group was housed under normal conditions and switched to individual housing only during the reversed light/dark cycle and noise phase. At week 6, CUMS model mice were randomized into subgroups to receive saline solution (vehicle), 15 mg/kg 5-MeO-DMT, and 15 mg/kg 5-OH-DMT for the next 1 week, respectively. The doses chosen were based on previous preclinical experiments by us and others [76,77]. Drugs were dissolved in saline solution containing 0.1% DMSO and disrupted by ultrasound and then immediately administered via intraperitoneal injection. Then, mice with 1-week administration were tested for all behaviors.

PCPA model and treatment

Mice were randomly divided into the following 6 groups: control, WAY100635, PCPA, PCPA + WAY100635, PCPA + 5-OH-DMT, and PCPA + 5-OH-DMT + WAY100635. Mice in the control group were fed with saline solution containing 0.1% DMSO (vehicle) for 3 d. Mice that were injected subcutaneously with 150 mg/kg PCPA twice daily for 3 d developed symptoms of depression. For pharmacological treatment, mice were treated with 15 mg/kg 5-OH-DMT via intraperitoneal injection for 3 d during PCPA procedures. For WAY100635 treatment, mice were injected intraperitoneally with 1 mg/kg WAY100635 for 3 d. PCPA, 5-OH-DMT, and WAY100635 were dissolved in saline solution containing 0.1% DMSO and disrupted by ultrasound. Then, mice were tested for all behaviors.

Behavior tests

Tail suspension test

Mice were suspended by placing adhesive tape 1 cm from the tail tip. The immobility time was recorded for the last 4 min of the total 6 min.

Forced swimming test

Mice were placed in a cylinder filled with water (23 ± 1 °C) for 6 min. The immobility time was recorded during the last 4 min of the test.

Sucrose preference test

Mice were habituated with 1% sucrose and water from 2 different bottles for 3 d. These 2 bottles were placed on randomly assigned sides of the cage every day to eliminate side preference. Then, each mouse had free access to 1% sucrose and water from 2 bottles for 3 h. The total volume of liquid consumed from each bottle was measured. Sucrose preference was calculated by the following formula: sucrose preference (%) = sucrose consumption/(sucrose + water consumption) × 100%.

Morris water maze test

The water maze was divided into 4 quadrants, and mice were trained to escape from water by swimming to the platform for 4 trials per day with different start points for 4 consecutive days. On day 5, the test was conducted and mice searched freely for 1 min starting from the opposite quadrant of the platform. The latencies to reach the platform and times cross target was recorded using the software Morris.

Open-field test

Mice were placed in the center of an open-field box. A total of 5-min video was recorded to observe the locomotor activity of mice. The total distance traveled in the field and the time spent in the center zone by mice were measured.

Side effect detection

Mice were given 25 mg/kg 5-MeO-DMT or 25 mg/kg 5-OH-DMT by intraperitoneal injection. Then, HTR and HLA were immediately tested. Mice were placed into the observation arena (25 × 25 × 40 cm) under low-light conditions. The number of head-twitch events and total distance were respectively recorded for 10 and 30 min. For the HTR test, the number of head twitches was examined by 2 observers blinded to the treatments via video recordings. For the HLA test, the total distance traveled was measured by using tracking software to process video recordings.

GloSensor cAMP assay

The downstream Gαi signaling of 5-HT_{1A} was assessed using the GloSensor cAMP assay (Promega). HEK 293T cells were cultured

in DMEM with 10% FBS and 1% penicillin–streptomycin at 37 °C and 5% CO_2. Cells were transfected with 5-HT_{1A} constructs and the GloSensor-22F biosensor at a 3:2 ratio. After 24 h, cells were resuspended in CO_2-independent medium with 2% GloSensor reagent and plated at 3.5×10^5 cells/ml (20 μl/well) into 384-well plates. After 1-h incubation, forskolin (1 μM) and test ligands were added, and luminescence was immediately recorded using an EnVision plate reader (PerkinElmer).

Inositol phosphate accumulation assay

The downstream Gαq signaling of 5-HT_{2A} was evaluated using the IP-One HTRF assay (Cisbio). HEK 293T cells were cultured in DMEM with 10% FBS and 1% penicillin–streptomycin at 37 °C, 5% CO_2. After 24 h of transfection, cells were resuspended in stimulation buffer (8×10^5 cells/ml) and plated at 7 μl/well into 384-well plates. Ligands diluted in buffer (7 μl) were added and incubated for 1 h at 37 °C. IP-One-d2 and anti-IP-One cryptate (3 μl each) were then added, followed by 30-min incubation at room temperature. HTRF signals were measured using an EnVision reader (PerkinElmer).

Statistical analysis

For all behavioral studies, mice were randomly assigned to the groups. In addition, investigators were blinded to the group until data had been collected. GraphPad Prism 9 was used to analyze all of the functional research data, and the results are provided as mean ± standard error of the mean from at least 3 separate trials. An evaluation of the concentration–response curves was carried out using a logistic equation with 3 parameters. Calculations of pEC_{50} values were performed with the use of the sigmoid 3-parameter equation. In order to assess the significance, a 1-way or 2-way analysis of variance was conducted, followed by Bonferroni's or Dunnett's post hoc test. Differences were considered significant when $P < 0.05$ and are shown as $^*P < 0.05$, $^{**}P < 0.01$, or $^{***}P < 0.001$.

Ethical Approval

All institutional and national guidelines regarding the care and use of animals were adhered to.

Acknowledgments

Some figures were created using resources from Servier Medical Art, licensed under Creative Commons Attribution 3.0 Unported License (https://creativecommons.org/licenses/by/3.0/). Cryo-EM data were collected at the Advanced Center for Electron Microscopy, Shanghai Institute of Materia Medica (SIMM), and we gratefully acknowledge the support of all staff involved in data acquisition.

Funding: This work was supported by the National Natural Science Foundation of China (Grant Nos. 82574558, 82404881, 82304743, and 82204715), the Postgraduate Research & Practice Innovation Program of Jiangsu Province, the Natural Science Foundation of Nanjing University of Chinese Medicine (No. XPT82304743), and the National-Level Integrated Traditional Chinese and Western Medicine "Flagship" Department Development Initiative (No. 2024-221).

Author contributions: S.L. designed the expression constructs, purified 5-HT_{1A} proteins, performed functional assays, and drafted the manuscript with input from all authors. Q.Y. handled cryo-EM data analysis and model building and contributed to supplementary figures and text. W.W. conducted animal experiments and assisted in figure and manuscript preparation. Z.C. and Y.Z. participated in animal studies. H.S. aided in model construction. K.W. and W.H. managed cryo-EM grid preparation and data collection. Q.C. performed molecular docking. J.Z. provided synthesized some compounds, L.H. provided plasmids, and Jia Duan conducted structural analysis and manuscript revision. The project was conceived and supervised by Jin-ao Duan, J.Z., H.E.X., and H.M.

Competing interests: The authors declare that they have no competing interests.

Data Availability

The data supporting this study are available from the corresponding authors upon reasonable request. Cryo-EM density maps have been deposited in the Electron Microscopy Data Bank under accession codes EMD-62593 (5-MeO-DMT), EMD-62595 (5-OH-DMT), and EMD-62594 (5-OH-TMT). The corresponding atomic coordinates are available in the Protein Data Bank under accession codes 9KVG, 9KVI, and 9KVH, respectively. Source data are provided with this paper.

Supplementary Materials

Figs. S1 to S10
Tables S1 to S3

References

1. Herrman H, Patel V, Kieling C, Berk M, Buchweitz C, Cuijpers P, Furukawa TA, Kessler RC, Kohrt BA, Maj M, et al. Time for united action on depression: A *Lancet*–World Psychiatric Association Commission. *Lancet*. 2022;399(10328):957–1022.
2. Guo M, Zhang H, Huang Y, Diao Y, Wang W, Li Z, Feng S, Zhou J, Ning Y, Wu F, et al. Transcriptional patterns of nodal entropy abnormalities in major depressive disorder patients with and without suicidal ideation. *Research*. 2025;8:0659.
3. Jakobsen JC, Katakam KK, Schou A, Hellmuth SG, Stallknecht SE, Leth-Møller K, Iversen M, Banke MB, Petersen IJ, Klingenberg SL, et al. Selective serotonin reuptake inhibitors versus placebo in patients with major depressive disorder. A systematic review with meta-analysis and Trial Sequential Analysis. *BMC Psychiatry*. 2017;17(1):58.
4. Fornaro M, Anastasia A, Novello S, Fusco A, Pariano R, De Berardis D, Solmi M, Veronese N, Stubbs B, Vieta E, et al. The emergence of loss of efficacy during antidepressant drug treatment for major depressive disorder: An integrative review of evidence, mechanisms, and clinical implications. *Pharmacol Res*. 2019;139:494–502.
5. Gaynes BN, Lux L, Gartlehner G, Asher G, Forman-Hoffman V, Green J, Boland E, Weber RP, Randolph C, Bann C, et al. Defining treatment-resistant depression. *Depress Anxiety*. 2020;37(2):134–145.
6. Massart R, Mongeau R, Lanfumey L. Beyond the monoaminergic hypothesis: Neuroplasticity and epigenetic changes in a transgenic mouse model of depression. *Philos Trans R Soc Lond B Biol Sci*. 2012;367(1601):2485–2494.
7. Slattery D, Hudson A, Nutt D. Invited review: The evolution of antidepressant mechanisms. *Fundam Clin Pharmacol*. 2004;18(1):1–21.

8. Yohn CN, Gergues MM, Samuels BA. The role of 5-HT receptors in depression. *Mol Brain*. 2017;10(1):28.
9. Sekssaoui M, Bockaert J, Marin P, Bécamel C. Antidepressant-like effects of psychedelics in a chronic despair mouse model: Is the 5-HT_{2A} receptor the unique player? *Neuropsychopharmacology*. 2024;49(4):747–756.
10. Drevets WC, Frank E, Price JC, Kupfer DJ, Greer PJ, Mathis C. Serotonin type-1A receptor imaging in depression. *Nucl Med Biol*. 2000;27(5):499–507.
11. Hirvonen J, Karlsson H, Kajander J, Lepola A, Markkula J, Rasi-Hakala H, Någren K, Salminen JK, Hietala J. Decreased brain serotonin 5-HT_{1A} receptor availability in medication-naive patients with major depressive disorder: An in-vivo imaging study using PET and [*carbonyl*-^{11}C]WAY-100635. *Int J Neuropsychopharmacol*. 2008;11(4):465–476.
12. Wu S, Comings D. A common C-1018G polymorphism in the human *5-HT_{1A}* receptor gene. *Psychiatr Genet*. 1999;9(2):105–106.
13. Klemenhagen KC, Gordon JA, David DJ, Hen R, Gross CT. Increased fear response to contextual cues in mice lacking the 5-HT1A receptor. *Neuropsychopharmacology*. 2006;31(1):101–111.
14. Ślifirski G, Król M, Turło J. 5-HT receptors and the development of new antidepressants. *Int J Mol Sci*. 2021;22.
15. Barros M, Mello EL Jr, Maior RS, Müller CP, de Souza Silva MA, Carey RJ, Huston JP, Tomaz C. Anxiolytic-like effects of the selective 5-HT_{1A} receptor antagonist WAY 100635 in non-human primates. *Eur J Pharmacol*. 2003;482(1–2):197–203.
16. Parks CL, Robinson PS, Sibille E, Shenk T, Toth M. Increased anxiety of mice lacking the serotonin$_{1A}$ receptor. *Proc Nat Acad Sci USA*. 1998;95(18):10734–10739.
17. Loane C, Politis M. Buspirone: What is it all about? *Brain Res*. 2012;1461:111–118.
18. Chauhan M, Parry R, Bobo WV. Vilazodone for major depression in adults: Pharmacological profile and an updated review for clinical practice. *Neuropsychiatr Dis Treat*. 2022;18:1175.
19. Wirth A, Holst K, Ponimaskin E. How serotonin receptors regulate morphogenic signalling in neurons. *Prog Neurobiol*. 2017;151:35–56.
20. Cipriani A, Furukawa TA, Salanti G, Chaimani A, Atkinson LZ, Ogawa Y, Leucht S, Ruhe HG, Turner EH, Higgins JPT, et al. Comparative efficacy and acceptability of 21 antidepressant drugs for the acute treatment of adults with major depressive disorder: A systematic review and network meta-analysis. *Lancet*. 2018;391(10128):1357–1366.
21. Hofmann SG, Curtiss J, Carpenter JK, Kind S. Effect of treatments for depression on quality of life: A meta-analysis. *Cogn Behav Ther*. 2017;46(4):265–286.
22. Locher C, Koechlin H, Zion SR, Werner C, Pine DS, Kirsch I, Kessler RC, Kossowsky J. Efficacy and safety of selective serotonin reuptake inhibitors, serotonin-norepinephrine reuptake inhibitors, and placebo for common psychiatric disorders among children and adolescents: A systematic review and meta-analysis. *JAMA Psychiatry*. 2017;74(10):1011–1020.
23. Wei W-L, Hou J-J, Wang X, Yu Y, Li H-J, Li Z-W, Feng Z-J, Qu H, Wu W-Y, Guo D-A. *Venenum bufonis*: An overview of its traditional use, natural product chemistry, pharmacology, pharmacokinetics and toxicology. *J Ethnopharmacol*. 2019;237:215–235.
24. Klein LM, Cozzi NV, Daley PF, Brandt SD, Halberstadt AL. Receptor binding profiles and behavioral pharmacology of ring-substituted *N*,*N*-diallyltryptamine analogs. *Neuropharmacology*. 2018;142:231–239.
25. Tittarelli R, Mannocchi G, Pantano F, Romolo FS. Recreational use, analysis and toxicity of tryptamines. *Curr Neuropharmacol*. 2015;13(1):26–46.
26. Bogenschutz MP, Ross S. Therapeutic applications of classic hallucinogens. *Curr Top Behav Neurosci*. 2018;36:361–391.
27. Heifets BD, Olson DE. Therapeutic mechanisms of psychedelics and entactogens. *Neuropsychopharmacology*. 2024;49:104–118.
28. Blough BE, Landavazo A, Decker AM, Partilla JS, Baumann MH, Rothman RB. Interaction of psychoactive tryptamines with biogenic amine transporters and serotonin receptor subtypes. *Psychopharmacology*. 2014;231(21):4135–4144.
29. Mayer FP, Niello M, Cintulova D, Sideromenos S, Maier J, Li Y, Bulling S, Kudlacek O, Schicker K, Iwamoto H, et al. Serotonin-releasing agents with reduced off-target effects. *Mol Psychiatry*. 2023;28(2):722–732.
30. Klein AK, Chatha M, Laskowski LJ, Anderson EI, Brandt SD, Chapman SJ, McCorvy JD, Halberstadt AL. Investigation of the structure–activity relationships of psilocybin analogues. *ACS Pharmacol Transl Sci*. 2020;4(2):533–542.
31. Cozzi NV, Daley PF. Receptor binding profiles and quantitative structure–affinity relationships of some 5-substituted-*N*,*N*-diallyltryptamines. *Bioorg Med Chem Lett*. 2016;26(3):959–964.
32. Arunotayanun W, Dalley JW, Huang X-P, Setola V, Treble R, Iversen L, Roth BL, Gibbons S. An analysis of the synthetic tryptamines AMT and 5-MeO-DALT: Emerging 'novel psychoactive drugs'. *Bioorg Med Chem Lett*. 2013;23(11):3411–3415.
33. Kwan AC, Olson DE, Preller KH, Roth BL. The neural basis of psychedelic action. *Nat Neurosci*. 2022;25(11):1407–1419.
34. Olson DE. The subjective effects of psychedelics may not be necessary for their enduring therapeutic effects. *ACS Pharmacol Transl Sci*. 2020;4(2):563–567.
35. Rosenblat JD, Leon-Carlyle M, Ali S, Husain MI, McIntyre RS. Antidepressant effects of psilocybin in the absence of psychedelic effects. *Am J Psychiatry*. 2023;180(5):395–396.
36. Kuypers KP, Ng L, Erritzoe D, Knudsen GM, Nichols CD, Nichols DE, Pani L, Soula A, Nutt D. Microdosing psychedelics: More questions than answers? An overview and suggestions for future research. *J Psychopharmacol*. 2019;33(9):1039–1057.
37. Warren AL, Lankri D, Cunningham MJ, Serrano IC, Parise LF, Kruegel AC, Duggan P, Zilberg G, Capper MJ, Havel V, et al. Structural pharmacology and therapeutic potential of 5-methoxytryptamines. *Nature*. 2024;630(8015):237–246.
38. Krebs-Thomson K, Ruiz EM, Masten V, Buell M, Geyer MA. The roles of 5-HT_{1A} and 5-HT_2 receptors in the effects of 5-MeO-DMT on locomotor activity and prepulse inhibition in rats. *Psychopharmacology*. 2006;189(3):319–329.
39. Halberstadt AL, Geyer MA. Multiple receptors contribute to the behavioral effects of indoleamine hallucinogens. *Neuropharmacology*. 2011;61(3):364–381.
40. Liang Y-L, Zhao P, Draper-Joyce C, Baltos J-A, Glukhova A, Truong TT, May LT, Christopoulos A, Wootten D, Sexton PM, et al. Dominant negative G proteins enhance formation and purification of agonist-GPCR-G protein complexes for structure determination. *ACS Pharmacol Transl Sci*. 2018;1(1):12–20.
41. Xu P, Huang S, Zhang H, Mao C, Zhou XE, Cheng X, Simon IA, Shen D-D, Yen H-Y, Robinson CV, et al. Structural

insights into the lipid and ligand regulation of serotonin receptors. *Nature*. 2021;592(7854):469–473.
42. Ballesteros J, Weinstein H. Integrated methods for the construction of three-dimensional models and computational probing of structure-function relations in G protein-coupled receptors. *Methods Neurosci*. 1995;25:366–428.
43. Han S, Li XX, Wei S, Zhao D, Ding J, Xu Y, Yu C, Chen Z, Zhou DS, Yuan TF. Orbitofrontal cortex-hippocampus potentiation mediates relief for depression: A randomized double-blind trial and TMS-EEG study. *Cell Rep Med*. 2023;4(6):Article 101060.
44. Eriksson PS, Perfilieva E, Björk-Eriksson T, Alborn AM, Nordborg C, Peterson DA, Gage FH. Neurogenesis in the adult human hippocampus. *Nat Med*. 1998;4(11):1313–1317.
45. Passchier J, van Waarde A, Pieterman RM, Elsinga PH, Pruim J, Hendrikse HN, Willemsen AT, Vaalburg W. In vivo delineation of 5-HT_{1A} receptors in human brain with [^{18}F] MPPF. *J Nucl Med*. 2000;41(11):1830–1835.
46. Blier P, Bergeron R, de Montigny C. Selective activation of postsynaptic 5-HT_{1A} receptors induces rapid antidepressant response. *Neuropsychopharmacology*. 1997;16(5):333–338.
47. Blier P, Ward NM. Is there a role for 5-HT_{1A} agonists in the treatment of depression? *Biol Psychiatry*. 2003;53(3):193–203.
48. Carhart-Harris RL, Nutt DJ. Serotonin and brain function: A tale of two receptors. *J Psychopharmacol*. 2017;31(9):1091–1120.
49. Price KL, Bower KS, Thompson AJ, Lester HA, Dougherty DA, Lummis SC. A hydrogen bond in loop A is critical for the binding and function of the 5-HT_3 receptor. *Biochemistry*. 2008;47(24):6370–6377.
50. Taliani S, Da Settimo F, Martini C, Laneri S, Novellino E, Greco G. Exploiting the indole scaffold to design compounds binding to different pharmacological targets. *Molecules*. 2020;25(10):2331.
51. Khemaissa S, Sagan S, Walrant A. Tryptophan, an amino-acid endowed with unique properties and its many roles in membrane proteins. *Crystals*. 2021;11(9):1032.
52. Zohairi F, Khandelia H, Zanjani AAH. Interaction of psychedelic tryptamine derivatives with a lipid bilayer. *Chem Phys Lipids*. 2023;251:Article 105279.
53. Shen H-W, Jiang X-L, Winter JC, Yu A-M. Psychedelic 5-methoxy-N,N-dimethyltryptamine: Metabolism, pharmacokinetics, drug interactions, and pharmacological actions. *Curr Drug Metab*. 2010;11(8):659–666.
54. Jayakodiarachchi N, Maurer MA, Schultz DC, Dodd CJ, Thompson Gray A, Cho HP, Boutaud O, Jones CK, Lindsley CW, Bender AM. Evaluation of the indazole analogs of 5-MeO-DMT and related tryptamines as serotonin receptor 2 agonists. *ACS Med Chem Lett*. 2024;15(2):302–309.
55. Chiodi D, Ishihara Y. The role of the methoxy group in approved drugs. *Eur J Med Chem*. 2024;273:Article 116364.
56. Jaster AM, González-Maeso J. Mechanisms and molecular targets surrounding the potential therapeutic effects of psychedelics. *Mol Psychiatry*. 2023;28:3595–3612.
57. McCorvy JD, Butler KV, Kelly B, Rechsteiner K, Karpiak J, Betz RM, Kormos BL, Shoichet BK, Dror RO, Jin J, et al. Structure-inspired design of β-arrestin-biased ligands for aminergic GPCRs. *Nat Chem Biol*. 2018;14:126–134.
58. González-Maeso J, Weisstaub NV, Zhou M, Chan P, Ivic L, Ang R, Lira A, Bradley-Moore M, Ge Y, Zhou Q. Hallucinogens recruit specific cortical 5-HT_{2A} receptor-mediated signaling pathways to affect behavior. *Neuron*. 2007;53(3):439–452.
59. Cameron LP, Benetatos J, Lewis V, Bonniwell EM, Jaster AM, Moliner R, Castrén E, McCorvy JD, Palner M, Aguilar-Valles A. Beyond the 5-HT_{2A} receptor: Classic and nonclassic targets in psychedelic drug action. *J Neurosci*. 2023;43(45):7472–7482.
60. Zhao C, Chen M, Sun SL, Wang JJ, Zhong Y, Chen HH, Li HM, Xu H, Li NG, Ma HY, et al. Bufotenine and its derivatives: Synthesis, analgesic effects identification and computational target prediction. *Chin J Nat Med*. 2021;19(6):454–463.
61. Chun E, Thompson AA, Liu W, Roth CB, Griffith MT, Katritch V, Kunken J, Xu F, Cherezov V, Hanson MA, et al. Fusion partner toolchest for the stabilization and crystallization of G protein-coupled receptors. *Structure*. 2012;20(6):967–976.
62. Wang C, Jiang Y, Ma J, Wu H, Wacker D, Katritch V, Han GW, Liu W, Huang X-P, Vardy E, et al. Structural basis for molecular recognition at serotonin receptors. *Science*. 2013;340(6132):610–614.
63. Zheng SQ, Palovcak E, Armache J-P, Verba KA, Cheng Y, Agard DA. MotionCor2: Anisotropic correction of beam-induced motion for improved cryo-electron microscopy. *Nat Methods*. 2017;14(4):331–332.
64. Rohou A, Grigorieff N. CTFFIND4: Fast and accurate defocus estimation from electron micrographs. *J Struct Biol*. 2015;192(2):216–221.
65. Punjani A, Rubinstein JL, Fleet DJ, Brubaker MA. cryoSPARC: Algorithms for rapid unsupervised cryo-EM structure determination. *Nat Methods*. 2017;14(3):290–296.
66. Wang JJ, Jin S, Zhang H, Xu Y, Hu W, Jiang Y, Chen C, Wang DW, Xu HE, Wu C. Molecular recognition and activation of the prostacyclin receptor by anti-pulmonary arterial hypertension drugs. *Sci Adv*. 2024;10(6):eadk5184.
67. Pettersen EF, Goddard TD, Huang CC, Couch GS, Greenblatt DM, Meng EC, Ferrin TE. UCSF Chimera—A visualization system for exploratory research and analysis. *J Comput Chem*. 2004;25(13):1605–1612.
68. Emsley P, Cowtan K. *Coot*: Model-building tools for molecular graphics. *Acta Crystallogr D Biol Crystallogr*. 2004;60:2126–2132.
69. Adams PD, Gopal K, Grosse-Kunstleve RW, Hung L-W, Ioerger TR, McCoy AJ, Moriarty NW, Pai RK, Read RJ, Romo TD, et al. Recent developments in the PHENIX software for automated crystallographic structure determination. *J Synchrotron Radiat*. 2004;11:53–55.
70. Croll TI. ISOLDE: A physically realistic environment for model building into low-resolution electron-density maps. *Acta Crystallogr D Biol Crystallogr*. 2018;74:519–530.
71. Pettersen EF, Goddard TD, Huang CC, Meng EC, Couch GS, Croll TI, Morris JH, Ferrin TE. UCSF ChimeraX: Structure visualization for researchers, educators, and developers. *Protein Sci*. 2021;30(1):70–82.
72. Gordon JC, Myers JB, Folta T, Shoja V, Heath LS, Onufriev A. H++: A server for estimating pK_as and adding missing hydrogens to macromolecules. *Nucleic Acids Res*. 2005;33:W368–W371.
73. Ramachandran S, Kota P, Ding F, Dokholyan NV. Automated minimization of steric clashes in protein structures. *Proteins*. 2011;79(1):261–270.
74. Trott O, Olson AJ. AutoDock Vina: Improving the speed and accuracy of docking with a new scoring function, efficient optimization, and multithreading. *J Comput Chem*. 2010;31(2):455–461.

75. Xu C, Liu J, Guo M, Wang J, Bai X, Zhang C, Luan X, Pei H, Liu H, Lv X, et al. Targeting ApoE–KCC2 signaling rescues GABAergic synaptic dysfunction and depression-like behaviors in mice. *Research*. 2025;8:0746.
76. Jefferson SJ, Gregg I, Dibbs M, Liao C, Wu H, Davoudian PA, Woodburn SC, Wehrle PH, Sprouse JS, Sherwood AM, et al. 5-MeO-DMT modifies innate behaviors and promotes structural neural plasticity in mice. *Neuropsychopharmacology*. 2023;48(9):1257–1266.
77. Jiang XL, Shen HW, Yu AM. Modification of 5-methoxy-*N*, *N*-dimethyltryptamine-induced hyperactivity by monoamine oxidase A inhibitor harmaline in mice and the underlying serotonergic mechanisms. *Pharmacol Rep*. 2016;68(3):608–615.